© 2019. Published by The Company of Biologists Ltd | Journal of Cell Science (2019) 132, jcs235580. doi:10.1242/jcs.235580

RESEARCH ARTICLE

# *Drosophila* emerins control LINC complex localization and transcription to regulate myonuclear position

**Torrey R. Mandigo, Blake D. Turcich, Alyssa J. Anderson, Michael R. Hussey and Eric S. Folker***

## ABSTRACT

Mispositioned nuclei are a hallmark of skeletal muscle disease. Many of the genes that are linked to Emery–Dreifuss muscular dystrophy (EDMD) encode proteins that are critical for nuclear movement in various cells, suggesting that disruptions in nuclear movement and position may contribute to disease progression. However, how these genes are coordinated to move nuclei is not known. Here, we focussed on two different emerin proteins in *Drosophila*, Bocksbeutel and Otefin, and their effects on nuclear movement. Although nuclear position was dependent on both, elimination of either Bocksbeutel or Otefin produced distinct phenotypes that were based in differential effects on the KASH-domain protein Klarsicht. Specifically, loss of Bocksbeutel reduced Klarsicht localization to the nucleus and resulted in a disruption in nuclear separation. Loss of Otefin increased the transcription of Klarsicht and led to premature separation of nuclei and their positioning closer to the edge of the muscle. Consistent with opposing functions, nuclear position is normal in *otefin*; *bocksbeutel* double mutants. These data indicate emerin-dependent regulation of Klarsicht levels in the nuclear envelope is a critical determinant of nuclear position.

**KEY WORDS: LINC complex, Emery–Dreifuss muscular dystrophy, Nuclear movement, Muscle development**

## INTRODUCTION

Skeletal muscle cells are characterized in part by the many nuclei that share a common cytoplasm. After the many nuclei are incorporated by iterative rounds of fusion, nuclei undergo a complex set of movements that leave them evenly spaced at the periphery of the cell. These movements are conserved throughout evolution (Folker and Baylies, 2013), and nuclei are mispositioned in the muscle cells of individuals with various muscle disorders (Dubowitz et al., 2007), suggesting that they are fundamental to muscle development.

One particular disease, Emery–Dreifuss muscular dystrophy (EDMD), is caused by mutations in a set of genes that encode proteins that mechanically link the nucleus to the cytoskeleton (Folker and Baylies, 2013; Crisp et al., 2006; Lombardi et al., 2011; Starr and Han, 2002). Many of the genes that are mutated in patients with EDMD encode for proteins that localize to the nucleus, including the inner nuclear membrane protein emerin, the structural nuclear protein lamin A/C, and proteins belonging to the linker of nucleoskeleton and cytoskeleton complex (LINC complex). The LINC complex is composed of SUN-domain proteins and KASH-domain proteins. SUN-domain proteins span the inner nuclear membrane and interact with the nucleoskeleton within the nucleus and with KASH-domain proteins in the lumen of the nuclear envelope. KASH-domain proteins span the outer nuclear membrane and interact with the cytoskeleton in the cytoplasm. Functionally, these proteins are critical for nuclear positioning in muscle cells (Roman and Gomes, 2018). Additionally, each gene is critical for nuclear movement in non-muscle cell types (Gundersen and Worman, 2013) indicating that regulation of nuclear movement is a fundamental function of EDMD-linked genes. However, how these individual components are coordinated to move nuclei is not known.

Emerin, the first identified cause of EDMD, is a LEM domain containing protein that is primarily localized to the inner nuclear membrane (Bione et al., 1994; Nagano et al., 1996; Manilal et al., 1996). LEM domain proteins interact with lamin and barrier-to-autointegration factor, and through these interactions can localize chromosomes to the nuclear periphery (Zheng et al., 2000; Cai et al., 2001; Laguri et al., 2001). Emerin also interacts with SUN1 and SUN2 (Haque et al., 2010) as well as short isoforms of KASH-domain proteins that localize to the inner nuclear envelope (Mislow et al., 2002; Wheeler et al., 2007). How each of these functions contributes to muscle development in general, or nuclear positioning during muscle development specifically, is not known. *Drosophila* provide an interesting system in which to study this mechanism as the *Drosophila* genome encodes only three LEM domain-containing proteins, MAN1, Bocksbeutel and Otefin (Ashery-Padan et al., 2015, 1997; Wagner et al., 2004, 2006; Pinto et al., 2008). *Drosophila* MAN1 is the homolog of mammalian LEM2 and MAN1 but both Bocksbeutel and Otefin are homologs of emerin (Wagner et al., 2006). Within the LEM domains Bocksbeutel and Otefin are 70% similar; however, outside of the LEM domain the similarity drops to 28% (Barton et al., 2014). Additionally, the expression patterns of these two emerin homologs differ, with uniform expression of Bocksbeutel throughout development, while Otefin is more highly expressed in embryos and first-instar larvae compared to later developmental stages (Wagner et al., 2006). The existence of two emerin-like proteins makes it possible that emerin functions are distributed between two separate proteins in *Drosophila* and therefore might simplify the process of understanding how each emerin function is coordinated and the contribution of each to muscle development.

We investigated the effects of emerin and other genes linked to EDMD during muscle development in *Drosophila* embryos and larvae (Collins et al., 2017). Consistent with previous reports, several EDMD-linked genes are critical for proper nuclear positioning (Elhanany-Tamir et al., 2012; Collins et al., 2017). Additionally, the *Drosophila* emerin homologs, *bocksbeutel* and *otefin*, both regulate nuclear position in embryonic and larval stages. However, the precise nuclear-positioning phenotypes that arise upon disruption of these genes differ. These differences are based

Department of Biology, Boston College, Chestnut Hill, MA 02467, USA.

*Author for correspondence (eric.folker@bc.edu)

E.S.F., 0000-0003-1619-7330

**Received 25 June 2019; Accepted 16 September 2019**

Journal of Cell Science (2019) 132, jcs235580. doi:10.1242/jcs.235580

on their distinct effects on the nuclear localization of the *Drosophila* KASH-domain protein, Klarsicht. Thus, nuclear level of Klarsicht is a critical regulator of nuclear positioning, which is differentially regulated by *bocksbeutel* and *otefin*.

## RESULTS

### Disruption of EDMD-linked genes impacts nuclear positioning in the *Drosophila* embryo

Like mammalian skeletal muscles, *Drosophila* body wall muscles contain many nuclei that are precisely positioned to maximize the distance between nuclei. Two EDMD-linked genes, *bocksbeutel* (*bocks*, a *Drosophila* emerin) and *klarsicht (klar*, a *Drosophila* KASH-domain protein), are known regulators of nuclear positioning in both embryonic and larval muscle (Elhanany-Tamir et al., 2012; Collins et al., 2017). Whether the effect on nuclear position in muscle is a conserved consequence of disrupting EDMD-linked genes or specific to those two genes is not clear. Furthermore, the genetic mechanism(s) by which these genes regulate nuclear position is not known. As a first step toward answering both questions, we measured nuclear position in flies with mutations that had previously not been characterized, namely *otefin* (*ote*, a *Drosophila* emerin) and *klaroid* (*koi*, the *Drosophila* SUN protein).

In stage 16 control embryos, nuclei were positioned in two equal-sized clusters with one near the dorsal end of the muscle and the other near the ventral end of the muscle (separated; equal distribution) (Fig. 1A,B). In $bocks^{DP01391}$ homozygous mutants and $klar^{1}$ homozygous mutants, nuclei remained as a single cluster near the ventral end of the muscle (clustered phenotype), spread through the center of the muscle with no distinct dorsal or ventral cluster (spread phenotype) or separated into two clusters of unequal size (separated; unequal distribution) as previously described (Fig. 1A,B) (Collins et al., 2017). In animals with the $ote^{DB}$ mutation, an amorphic allele caused by a nonsense mutation (Barton et al., 2013) that had not previously been investigated with respect to nuclear positioning, nuclei separated into two clusters. However there was an increase in the frequency of nuclei found in the center of the muscle (central phenotype) (Fig. 1A,B). In animals with the $koi^{EY03560}$ mutation, an allele with a p-element insertion in an early intron of *koi* (Technau and Roth, 2008) previously uninvestigated with respect to nuclear positioning, nuclei remained as a single cluster or separated into two clusters of unequal size as was seen in $bocks^{DP01391}$ and $klar^{1}$ mutants (Fig. 1A,B).

We also measured the distance from the dorsal and ventral ends of muscles to the nearest nucleus. Compared to controls, nuclei were positioned 63%, 59% and 48% further away from the dorsal muscle end in $bocks^{DP01391}$, $klar^{1}$ and $koi^{EY03560}$ embryos, respectively. Additionally, compared to controls, nuclei were positioned 11%, 12% and 15% closer to the ventral end of the muscle. Conversely, compared to controls, nuclei were positioned 11% closer to the dorsal muscle end in $ote^{DB}$ embryos (Fig. 1C,D). Crossing each mutant allele to a deficiency replicated the nuclear positioning defects observed in homozygous mutants (Fig. S1A–D), except for $bocks^{DP01391/Df}$, which had a high frequency of fusion defects and missing muscles (Fig. S1A). Owing to the muscle defects in $bocks^{DP01391/Df}$ embryos, only embryos with properly formed muscles were analyzed for nuclear positioning, leading to a bias in analysis of healthier embryos. Together, these data indicate that *bocksbeutel*, *klarsicht* and *klaroid* have a similar effect on nuclear positioning but that *otefin* has unique effects on nuclear position.

### Disruption of EDMD-linked genes impacts nuclear positioning in the *Drosophila* larvae

To test whether the disruptions in nuclear positioning persist through larval development, we measured nuclear distribution in $bocks^{DP01391}$, $klar^{1}$, $ote^{DB}$ and $koi^{EY03560}$ mutant L3 larvae as previously described (Collins et al., 2017). In controls, nuclei were typically positioned in two parallel lines on the long axis of the muscle (Fig. 1E) with an internuclear distance ratio (actual distance as a proportion of maximal distance) of 0.75 (Fig. 1F). In $bocks^{DP01391}$ and $klar^{1}$ larvae, nuclei formed a single line in the center of the muscle as previously described (Fig. 1E) (Collins et al., 2017), which phenocopied what was seen in *klar*-null larvae (Ding et al., 2017). The internuclear distance ratio was 0.57 and 0.58 for $bocks^{DP01391}$ and $klar^{1}$ larvae, respectively (Fig. 1F). Nuclear positioning in $koi^{EY03560}$ larvae phenocopied $bocks^{DP01391}$ and $klar^{1}$ larvae with a single line of nuclei positioned in the center of the muscle (Fig. 1E) with an internuclear distance ratio of 0.6 (Fig. 1F). Additionally, nuclei in $bocks^{DP01391}$, $klar^{1}$ and $koi^{EY03560}$ larvae were all positioned further from the muscle edge compared to controls (Fig. 1G). It has been previously demonstrated that nuclear positioning relative to the muscle edge scales with cell width (Windner et al., 2019). Therefore, we measured the average width of VL3 muscles and found that there was no significant difference between the average width of control, $bocks^{DP01391}$, $klar^{1}$ and $koi^{EY03560}$ muscles (Fig. 2A) suggesting that the observed nuclear positioning defects are not a consequence of thinner muscles and instead are bona fide disruptions in nuclear positioning.

To further investigate these nuclear positioning disruptions, we analyzed the relationship between the average distance of nuclei from the muscle edge as a function of muscle width. The slope of the line fit to the control data was nearly zero (Fig. 2B,C,F), indicating that the nuclei maintain a relatively constant distance from the edge of the muscle regardless of the muscle size. In $bocks^{DP01391}$, $klar^{1}$ and $koi^{EY03560}$ animals, nuclei were positioned further from the muscle edge as the muscle widened, indicating that nuclei had lost the ability to separate into two lines and maintain the proper distance from the muscle edge (Fig. 2C–F,H). The similarities in all measurements of nuclear position between *bocksbeutel*, *klarsicht* and *klaroid* mutants suggest that these genes regulate nuclear positioning through a common mechanism.

In contrast, the spacing between nuclei in $ote^{DB}$ larvae was similar to controls. However, in some regions of the muscle there were three lines of offset nuclei (Fig. 1E, yellow box). This resulted in disrupted nuclear positioning relative to the muscle edge (Fig. 1G), but proper spacing of nuclei relative to other nuclei (Fig. 1F). Additionally, as muscle width increased, the distance between the muscle edge and the nuclei scaled similarly to controls (Fig. 2G). This indicates that although nuclei were closer to the muscle edge in $ote^{DB}$ mutants, the effect is not caused by a difference in muscle width.

Crossing each mutant allele to a deficiency replicated the nuclear positioning defects observed in homozygous mutants (Fig. S1E–G), with the exception of $ote^{DB/Df}$. $ote^{DB/Df}$ had more severe nuclear positioning defects compared to homozygous mutant larvae, possibly due to the additional genes affected by the deficiency. Therefore, to confirm that the *ote* mutation caused the nuclear positioning defects, we examined trans-heterozygotes of two distinct *ote* alleles. Similar to $ote^{DB}$ homozygote larvae, the internuclear distance in $ote^{DB/B279}$ larvae was similar to controls, but nuclei were significantly closer to the edge of the muscle than in controls (Fig. S2A–C). That the disruption of *otefin* expression caused a distinct phenotype in homozygous and trans-heterozygous

Journal of Cell Science (2019) 132, jcs235580. doi:10.1242/jcs.235580

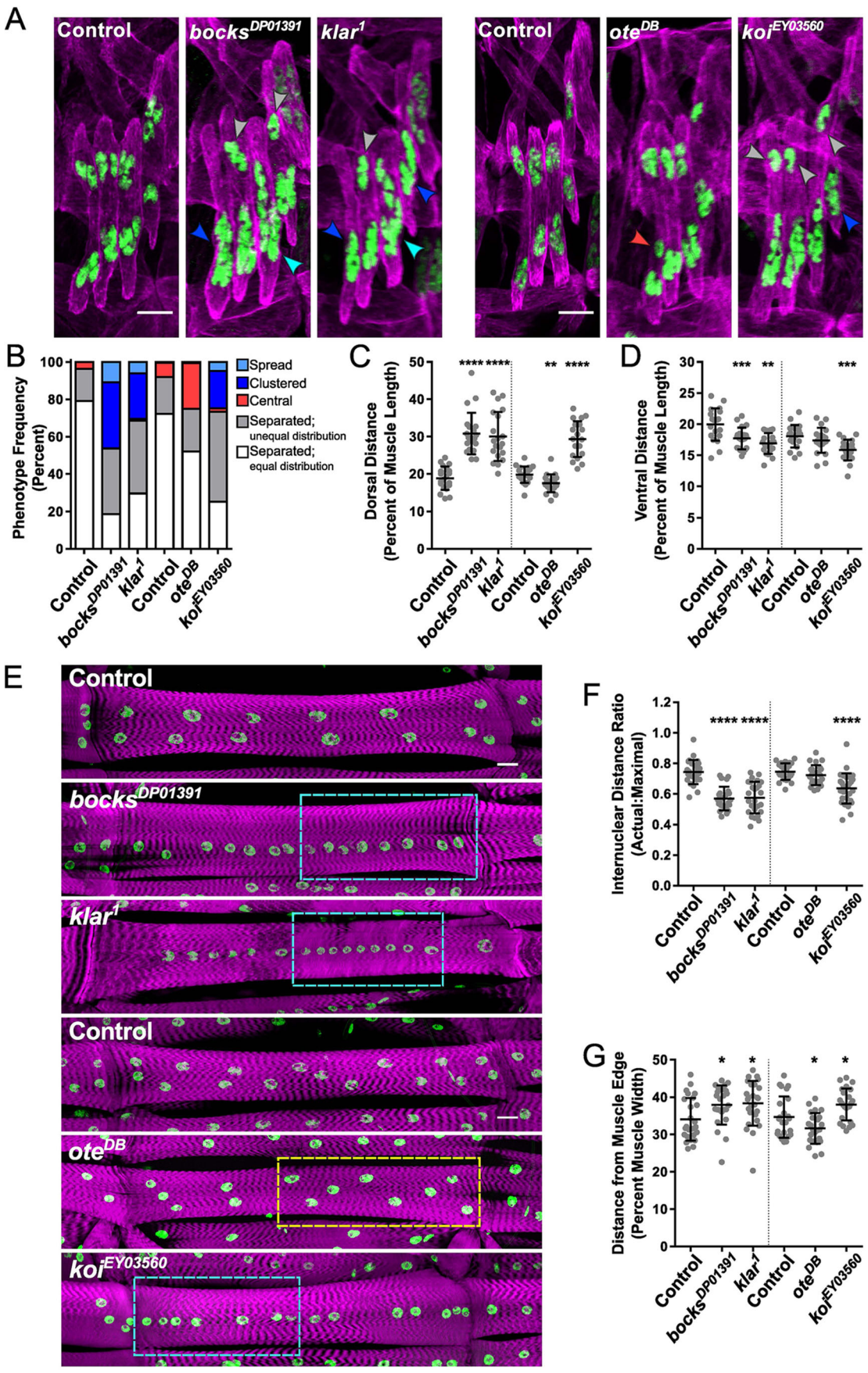


**Fig. 1.** See next page for legend.

**Fig. 1. The EDMD-linked genes *bocksbeutel*, *klarsicht*, *otefin* and *klaroid* are necessary for proper myonuclear positioning in *Drosophila* embryos and larvae.** (A) Immunofluorescence projection images of lateral transverse (LT) muscles in one hemisegment from stage 16 (16 h AEL) embryos of indicated genotypes. Magenta, Tropomyosin/muscles; green, dsRed/nuclei. Arrowheads indicate disrupted nuclear-positioning phenotypes. Dark blue, clustered nuclear positioning; gray, unequal separation of nuclear clusters; light blue, spread nuclear positioning; red, central nuclei. Scale bars: 10 µm. Separate controls [*Twist-GAL4*, *apRed* (control in first panel) and *DMef2-GAL4*, *apRed* (control in fourth panel)] were used to control for variations caused by differences in genetic background. (B) Qualitative analysis of the frequency at which nuclear-positioning phenotypes occur in the indicated genotypes. (C,D) Distance between the dorsal end of the muscle and the nearest nucleus (C) and between the ventral end of the muscle and the nearest nucleus (D) for the indicated genotypes normalized to muscle length. Each data point represents the average distances from all measured muscles within a single embryo. Error bars indicate the s.d. from 20 embryos. (E) Immunofluorescence projection images of ventral longitudinal 3 (VL3) muscles from dissected L3 larvae of the indicated genotype. Magenta, phalloidin/muscles; green, Hoechst/nuclei. Dashed boxes indicate disrupted nuclear-positioning phenotypes; light blue, single-file nuclei; yellow, three lines of offset nuclei with nuclei closer to the muscle edge. Scale bars: 25 µm. Separate controls [*Twist-GAL4*, *apRed* (control in first panel) and *DMef2-GAL4*, *apRed* (control in fourth panel)] were used to control for variations caused by differences in genetic background. (F) The ratio of actual internuclear distance to maximal internuclear distance in larval muscles from the indicated genotypes. Data points indicate the average value for the internuclear distance ratio for all nuclei within a single VL3 muscle. Error bars indicate the s.d. from 24 VL3 muscles. (G) The distance between nuclei and the nearest muscle edge in larval muscles from the indicated genotypes. Data points indicate the average distance from the muscle edge for all nuclei within a single VL3 muscle. Error bars indicate the s.d. from 24 VL3 muscles. **P*<0.05, ***P*<0.01, ****P*<0.001, *****P*<0.0001 compared to controls (Student's *t*-test).

mutants further indicates that *otefin* regulates nuclear positioning differently from *bocksbeutel*, *klarsicht* and *klaroid*.

### *Bocksbeutel* and *klarsicht* genetically interact to regulate nuclear positioning during muscle development

Since $bocks^{DP01391}$ mutants share nuclear-positioning phenotypes with $klar^{1}$ and $koi^{EY03560}$ mutants, we investigated whether *bocksbeutel* and the other *Drosophila* emerin homolog, *otefin*, genetically interact with other EDMD-linked genes to regulate nuclear positioning during embryonic and larval muscle development. In $bocks^{DP01391}$/+, $klar^{1}$/+ doubly heterozygous embryos, the frequencies of clustered nuclei, spread nuclei and two separate clusters of unequal size were increased compared to what was seen in either individual heterozygote (Fig. 3A,B). Additionally, the distance between the dorsal muscle end and the nearest nucleus was increased relative to that in each individual heterozygote (Fig. 3C), and the distance between the ventral end of the muscle and the nearest nucleus was decreased compared to each individual heterozygote (Fig. 3D). In $bocks^{DP01391}$/+, $klar^{1}$/+ doubly heterozygous larvae, nuclei formed a single line positioned in the center of the muscle, parallel to the long axis of the muscle. This phenotype was absent from each of the individual heterozygotes, although some regions of $bock^{DP01391}$/+ and $klar^{1}$/+ single heterozygote larval muscles contained single-file nuclei (Fig. 3E). Quantitatively, the internuclear distance ratio was significantly reduced in $bocks^{DP01391}$/+, $klar^{1}$/+ doubly heterozygous larval muscles compared to either individual heterozygote (Fig. 3F). Nuclei were also further from the muscle edge in $bocks^{DP01391}$/+, $klar^{1}$/+ double heterozygotes compared to each individual heterozygote (Fig. 3G). No genetic interactions were found between $bocks^{DP01391}$ and either $ote^{DB}$ or $koi^{EY03560}$ in embryonic (Fig. S3A–F) or larval (Fig. S4A–E) muscles. Additionally, no genetic interactions were found between $ote^{DB}$ and $klar^{1}$ and $koi^{EY03560}$ in embryonic (Fig. S3G–L) or larval (Fig. S4F–J) muscles. The genetic interaction between *bocksbeutel* and *klarsicht* suggests that Klarsicht may be a differentiating factor between the distinct mechanisms used to regulate nuclear positioning by Bocksbeutel and Otefin.

### Disruption of EDMD-linked genes affect the levels of nuclear-localized Klarsicht

In order to better understand the genetic interaction between *bocksbeutel* and *klarsicht*, we examined Klarsicht localization in $bocks^{DP01391}$ and $klar^{1}$ mutants. In both $bocks^{DP01391}$ and $klar^{1}$ mutants, nuclear Klarsicht levels were reduced compared to those in controls (Fig. 4A,B). Combined with the similar nuclear-positioning phenotype in both *bocksbeutel* and *klarsicht* mutants, these data suggest that Bocksbeutel contributes to nuclear position by regulating the levels of Klarsicht in the nuclear envelope. Similarly, in $koi^{EY03560}$ mutants, which exhibit nuclear positioning defects similar to those in $bocks^{DP01391}$ and $klar^{1}$ (Fig. 1A–G), nuclear Klarsicht levels were also reduced compared to controls (Fig. 4A,B). Conversely, in $ote^{DB}$ mutants, which are phenotypically distinct from $bocks^{DP01391}$, $klar^{1}$ and $koi^{EY03560}$ (Fig. 1A–G), nuclear Klarsicht levels were increased compared to controls (Fig. 4A,B). These data, combined with the clustering phenotype in embryonic muscles and the single-file nuclear-positioning phenotype in larval muscles being phenocopied in our $klar^{1/Df}$ mutant (Fig. S1E–G) and upon muscle-specific knockdown of *klar* by RNAi (Collins et al., 2017), suggest that these nuclear-positioning phenotypes result from a reduction in Klarsicht in the nuclear envelope, while the central nucleus phenotype in embryonic muscles and nuclei positioning closer to the edge in larval muscles results from an increase in Klarsicht in the nuclear envelope. To test the latter hypothesis, we overexpressed Klarsicht. Overexpressed Myc-tagged Klarsicht localized to the nuclear envelope and, similar to what was seen with the $ote^{DB}$ mutation, caused nuclei to be positioned closer to the edge of the muscle compared to controls (Fig. 5A–D). These data further suggest that reduced Otefin levels disrupt nuclear position by causing an increase in Klarsicht in the nuclear envelope.

Because the LINC complex and emerin can either directly or indirectly regulate transcriptional activity (Lee et al., 2001; Wilkinson et al., 2003; Holaska and Wilson, 2007; Navarro et al., 2016), we investigated the transcript levels of EDMD-linked genes in each mutant to determine whether nuclear Klarsicht levels changed due to altered transcription or altered protein localization. All transcript levels were the same in $bocks^{DP01391}$ mutants and controls. In particular, there was no change in *klar* transcript levels (Fig. 4C), suggesting that the decreased Klarsicht immunofluorescence represented a change in its localization. Additionally, no changes in EDMD-linked genes were observed at the transcript level in $klar^{1}$ mutants compared to controls (Fig. 4D). However, in $ote^{DB}$ mutants there was an increase in *klar* transcript levels compared to controls (Fig. 4E) suggesting that the increase in nuclear Klarsicht levels is caused by an increase in transcription of the *klar* gene. Additionally, in $koi^{EY03560}$ mutants, there was a significant increase in *bocks* transcript levels compared to controls (Fig. 4F) suggesting that SUN protein levels contribute to the regulation of emerin gene transcription.

### Loss of *otefin* rescues nuclear positioning defects caused by disruption of *bocksbeutel*

Since $bocks^{DP01391}$ homozygous mutants and $ote^{DB}$ homozygous mutants have different effects on nuclear Klarsicht levels, we investigated whether the functions of Bocksbeutel and Otefin

Journal of Cell Science (2019) 132, jcs235580. doi:10.1242/jcs.235580

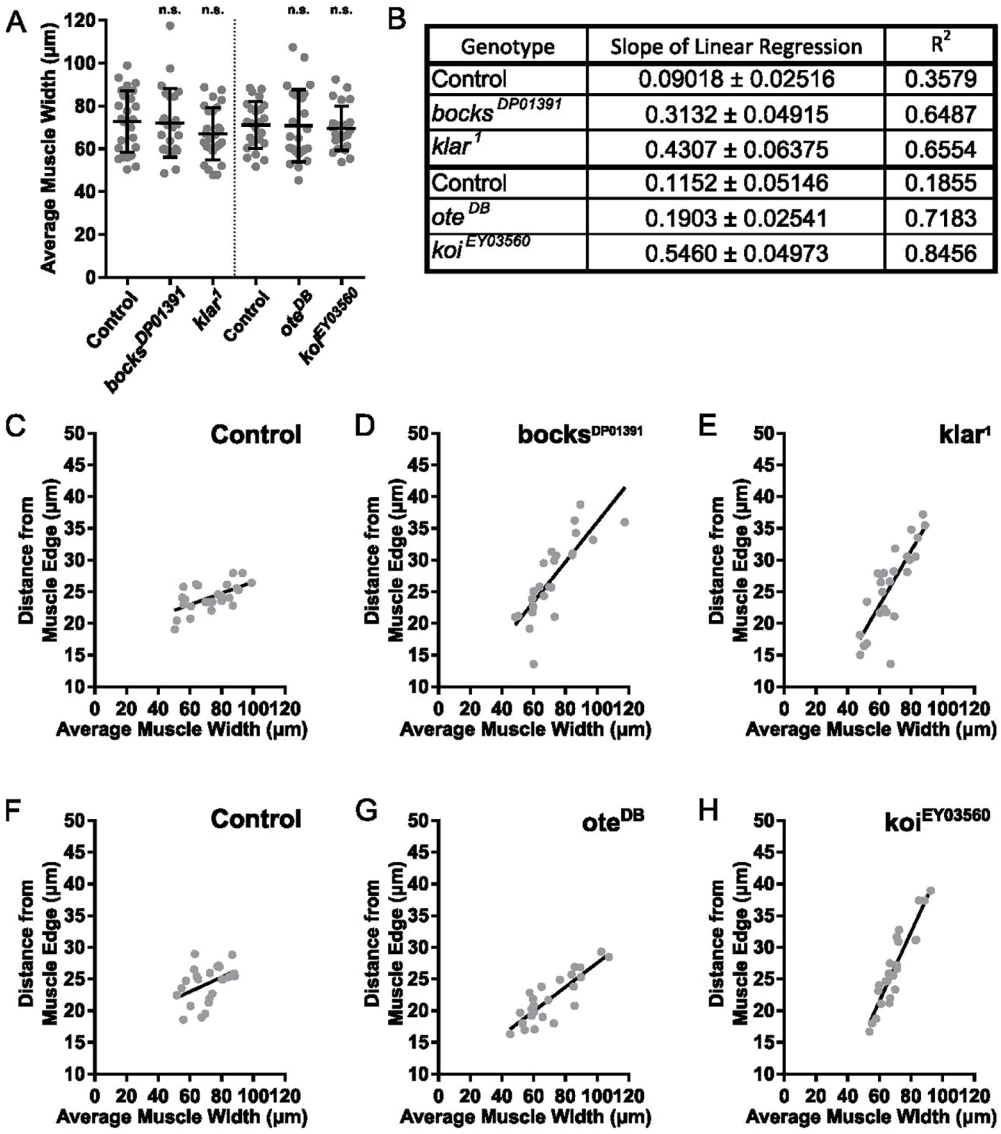


| Genotype | Slope of Linear Regression | $R^2$ |
|---|---|---|
| Control | 0.09018 ± 0.02516 | 0.3579 |
| *bocks*$^{DP01391}$ | 0.3132 ± 0.04915 | 0.6487 |
| *klar*$^{1}$ | 0.4307 ± 0.06375 | 0.6554 |
| Control | 0.1152 ± 0.05146 | 0.1855 |
| *ote*$^{DB}$ | 0.1903 ± 0.02541 | 0.7183 |
| *koi*$^{EY03560}$ | 0.5460 ± 0.04973 | 0.8456 |

**Fig. 2. The EDMD-linked genes *bocksbeutel*, *klarsicht*, *otefin* and *klaroid* affect the scaling of nuclear position relative to muscle edge.** (A) Average muscle width of VL3 muscles from dissected L3 larvae in the indicated genotypes. n.s., not significant ($P$>0.05). (B) Slope and $R^2$ values of the linear regressions for each dataset. (C–H) Distance from the muscle edge as a function of average muscle width of VL3 muscles from dissected L3 larvae of the indicated genotypes. Solid black line represents linear regression of the dataset. Separate controls [*Twist-GAL4*, *apRed* (C) and *DMef2-GAL4*, *apRed* (F)] were used to control for variations caused by differences in genetic background.

counterbalance each other to regulate nuclear positioning. In *bocks*$^{DP01391}$ larvae (Figs 1E and 5E), nuclei formed a single line positioned in the center of the muscle, parallel to the long axis of the muscle. When a single copy of the *ote*$^{DB}$ mutant allele was placed in a *bocks*$^{DP01391}$ homozygous mutant, there was a partial rescue of nuclear positioning with the internuclear distance ratio being 0.71 compared to 0.56 in the *bocks*$^{DP01391}$ homozygous mutant controls (Fig. 5E,F). Nuclear positioning was completely rescued in *ote*$^{DB}$*; bocks*$^{DP01391}$ larvae as nuclei formed two parallel lines along the long axis of the muscle (Fig. 5E) with an internuclear distance ratio of 0.78 (Fig. 5F). Additionally, the positioning relative to the muscle edge was rescued in *ote*$^{DB}$/+; *bocks*$^{DP01391}$ and *ote*$^{DB}$; *bocks*$^{DP01391}$ (Fig. 5G). Furthermore, the levels of nuclear-localized Klarsicht were rescued to control levels in *ote*$^{DB}$*; bocks*$^{DP01391}$ double mutants (Fig. 5H,I). These data suggest that Bocksbeutel and Otefin have opposing functions in regulating nuclear positioning and balancing these functions is necessary to properly position myonuclei and regulate nuclear Klarsicht levels.

## DISCUSSION

We have used *Drosophila* musculature to elucidate the genetic network and cellular mechanisms that regulate myonuclear position *in vivo*. Consistent with previous work, disruption of EDMD-linked genes caused mispositioned nuclei. Deeper characterization revealed that disruption of *bocksbeutel* (a *Drosophila emerin*), *klarsicht* (a *Drosophila* KASH-domain protein) and *klaroid* (the *Drosophila* SUN) caused a similar phenotype. However, disruption of *otefin*, the other *Drosophila* emerin homolog caused a different nuclear-positioning phenotype. Furthermore, *bocks*, but not *ote*, genetically interacted with *klar* to regulate nuclear positioning. The distinct phenotypes and genetic interactions of *bocks* and *ote* suggest a division of emerin functions between the two *Drosophila* emerin homologs.

Mechanistically, the phenotypic differences between *bocks* and *ote* mutants correlate with distinct changes in nuclear-localized Klarsicht. Disruption in *bocks* leads to a decrease in nuclear-localized Klarsicht while disruption in *ote* leads to an increase in nuclear-localized Klarsicht. Disruption of *bocks* caused no effect on transcript levels of *klar*, suggesting that the decrease in nuclear Klarsicht is due to mislocalization of Klarsicht. Conversely, disruption in *ote* caused an increase in transcript levels of *klar*, suggesting the increase in nuclear-localized Klarsicht is due to an increase in transcription. Although the increase in transcript levels is modest, it is important to note that quantitative PCR (qPCR) was

Journal of Cell Science (2019) 132, jcs235580. doi:10.1242/jcs.235580

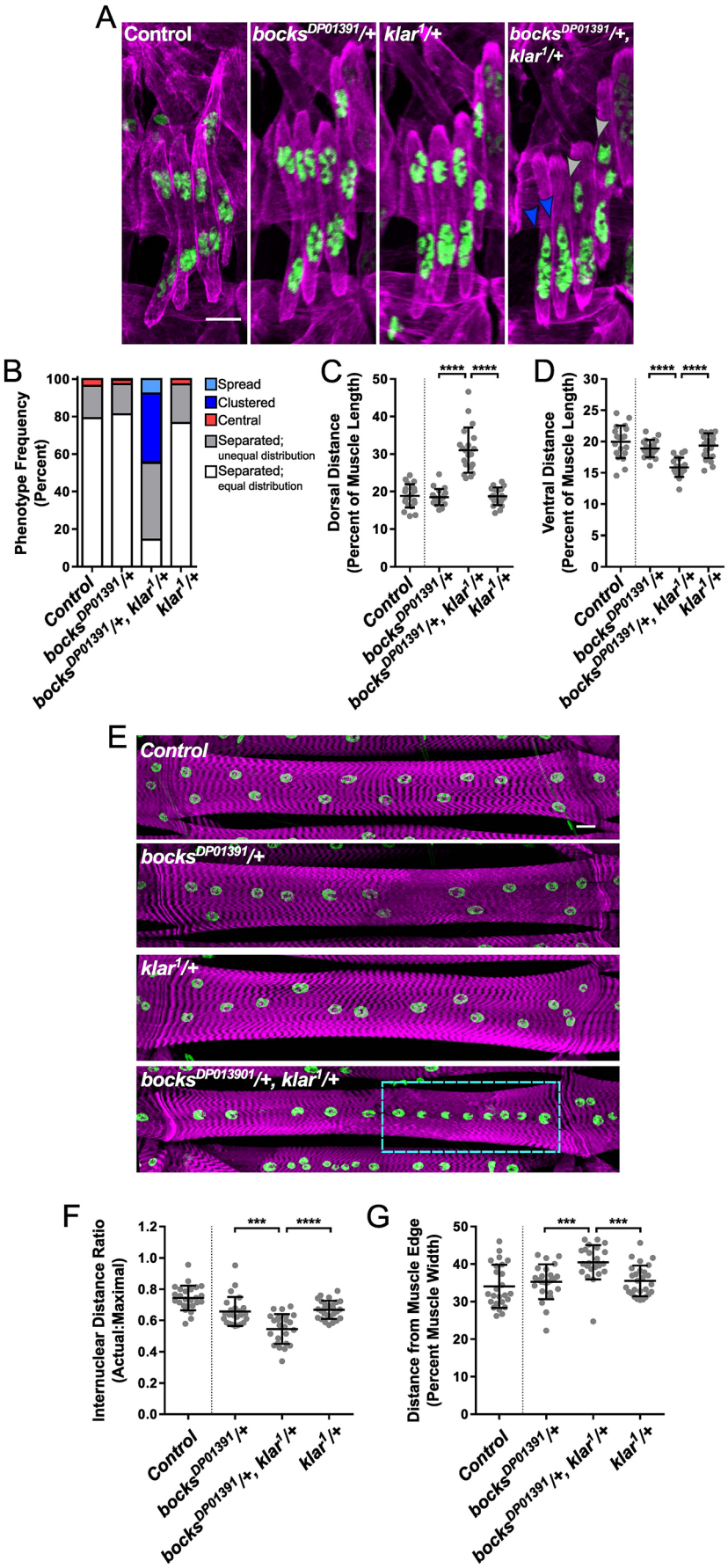


**Fig. 3. *bocksbeutel* genetically interacts with *klarsicht* to regulate nuclear positioning in embryonic and larval muscles.** (A) Immunofluorescence projection images of LT muscles in one hemisegment from stage 16 (16 h AEL) embryos with the indicated genotypes. Magenta, Tropomyosin/muscles; green, dsRed/nuclei. Arrowheads indicate disrupted nuclear-positioning phenotypes. dark blue, clustered nuclear positioning; gray, unequal separation of nuclear clusters. Scale bar: 10 µm. *Twist-GAL4*, *apRed* was used as a control. (B) Qualitative analysis of the frequency at which nuclear-positioning phenotypes occur in the indicated genotypes. (C,D) Distance between the dorsal end of the muscle and the nearest nucleus (C) and between the ventral end of the muscle and the nearest nucleus (D) for the indicated genotypes normalized to muscle length. Each data point represents the average distance for all muscles measured within a single embryo. Error bars indicate the s.d. from 20 embryos. (E) Immunofluorescence projection images of VL3 muscles from dissected L3 larvae of the indicated genotype. Magenta, phalloidin/muscles; green, Hoechst/nuclei. The dashed light blue box indicates the single-file disrupted nuclear-positioning phenotype. Scale bar: 25 µm. *Twist-GAL4*, *apRed* was used as a control. (F) The ratio of actual internuclear distance to maximal internuclear distance in larval muscles from the indicated genotypes. Data points indicate the average value for the internuclear distance ratio for all nuclei within a single VL3 muscle. Error bars indicate the s.d. from 24 VL3 muscles. (G) The distance between nuclei and the nearest muscle edge in larval muscles from the indicated genotypes. Data points indicate the average distance from the muscle edge for all nuclei within a single VL3 muscle. Error bars indicate s.d. from 24 VL3 muscles. ***$P$<0.001, ****$P$<0.0001 compared to controls (Student's $t$-test).

Journal of Cell Science (2019) 132, jcs235580. doi:10.1242/jcs.235580

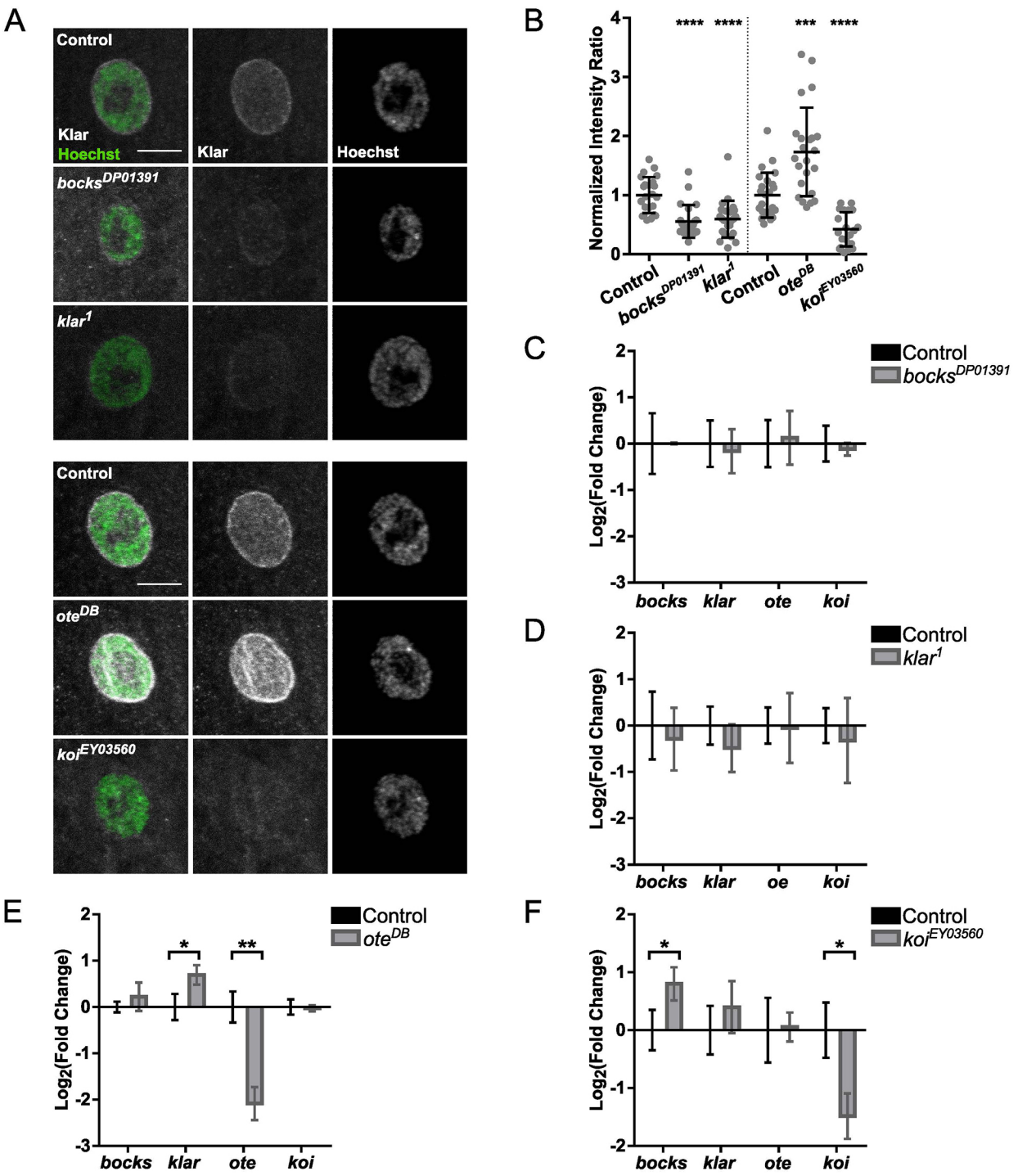


**Fig. 4. The EDMD-linked genes *bocksbeutel*, *otefin* and *klaroid* affect levels of nuclear-localized Klarsicht.** (A) Left, overlay of immunofluorescence images of nuclei in VL3 muscles from dissected L3 larvae of the indicated genotype. Gray, Klarsicht; green, Hoechst/nuclei. Scale bars: 10 µm. Middle and right, grayscale images of Klarsicht (middle) and Hoechst/nuclei (right) signals. Separate controls [*Twist-GAL4, apRed* (control in top row) and *DMef2-GAL4, apRed* (control in fourth row)] were used to control for variations caused by differences in genetic background. (B) Intensity ratio for average Klarsicht immunofluorescence, with background fluorescence subtracted, normalized to the maximum Hoechst immunofluorescence and nuclear size. Error bars indicate s.d. from at least 20 nuclei. (C–F) Gene expression as determined by qPCR of EDMD-linked genes in *bocks*$^{DP01391}$ (C), *klar*$^{1}$ (D), *ote*$^{DB}$ (E) and *koi*$^{EY01391}$ (F) normalized to levels of RP49, GAPDH and αTub84b. Gene expression is represented as fold change relative to that in *twist-GAL4*, *apRed* (C,D) or *DMef2-GAL4*, *apRed* (E,F) controls. Error bars indicate s.d. from three biological replicates. **P*<0.05, ***P*<0.01, ****P*<0.001, *****P*<0.0001 compared to control (Student's *t*-test).

conducted on whole-larval lysates. Therefore, if the phenotype were specific to a subset of tissues, or perhaps muscle specific, this would explain the modest change in transcript levels we observed. Together, these data suggest that *bocks* and *ote* serve unique functions in *Drosophila* abdominal muscles, but that both functions are critical to the regulation of nuclear positioning.

Nesprins and emerin have previously been shown to interact physically. However, these interactions were demonstrated

Journal of Cell Science (2019) 132, jcs235580. doi:10.1242/jcs.235580

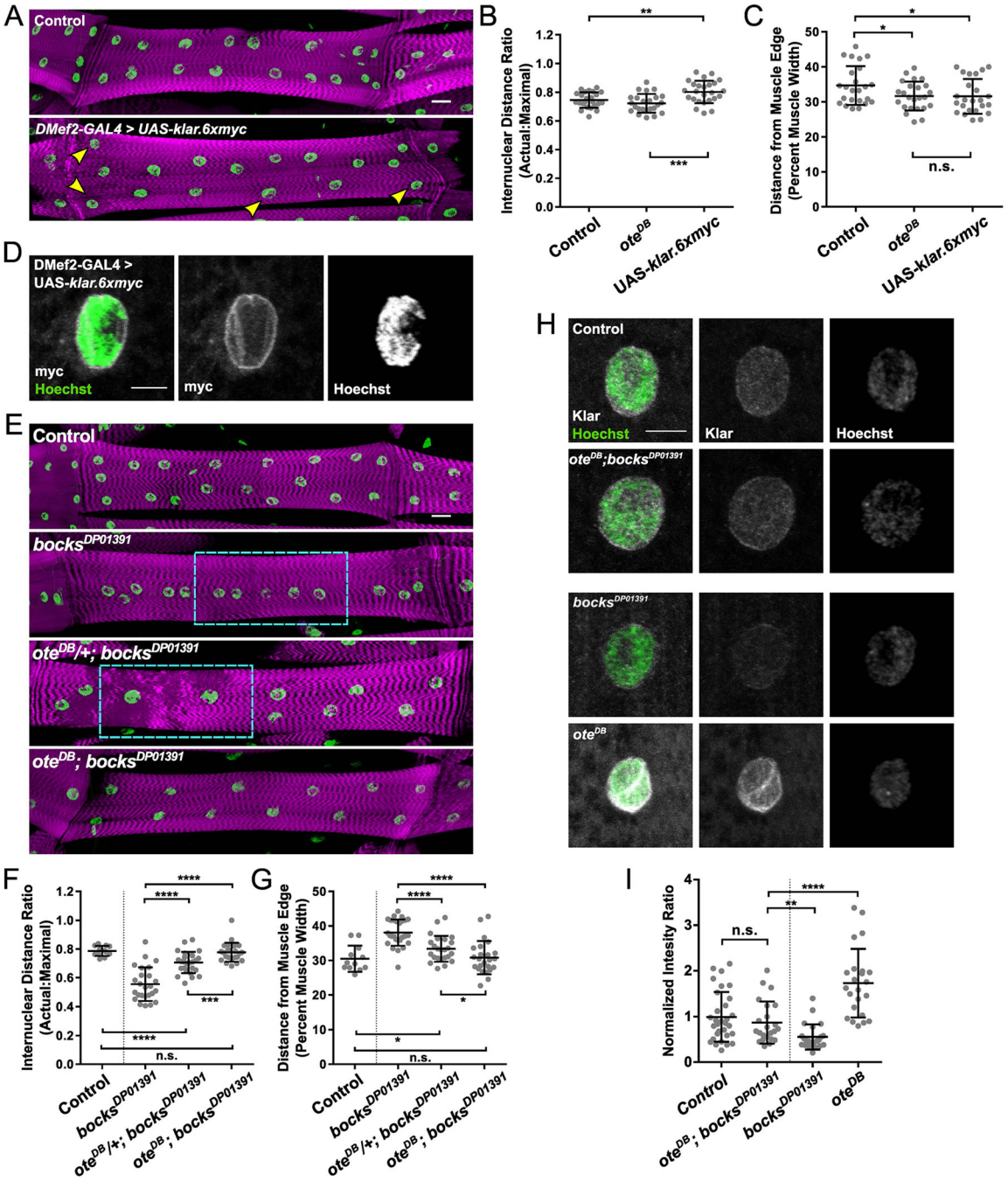


**Fig. 5. Loss of *otefin* rescues the nuclear-positioning phenotype caused by disruption of *bocksbeutel* and restores nuclear-localized Klarsicht to control levels.** (A) Immunofluorescence projection images of VL3 muscles from dissected L3 larvae of the indicated genotype. Magenta, phalloidin/muscles; green, Hoechst/nuclei. Yellow arrowheads indicate nuclei that are closer to the muscle edge. Scale bar: 25 µm. *DMef2-GAL4*, *apRed* was used as a control. (B) The ratio of actual internuclear distance to maximal internuclear distance in larval muscles from the indicated genotypes. Data points indicate the average value for the internuclear distance ratio for all nuclei within a single VL3 muscle. Error bars indicate the s.d. from 24 VL3 muscles. (C) The distance between nuclei and the nearest muscle edge in larval muscles from the indicated genotypes. Data points indicate the average distance from the muscle edge for all nuclei within a single VL3 muscle. Error bars indicate the s.d. from 24 VL3 muscles. (D) Left, overlay immunofluorescence images of nuclei in VL3 muscles from dissected L3 larvae of the indicated genotype. Gray, Myc; green, Hoechst/nuclei. Scale bar: 10 µm. Middle and right, grayscale images of Myc (middle) and Hoechst/nuclei (right). (E) Immunofluorescence projection images of VL3 muscles from dissected L3 larvae of the indicated genotype. Magenta, phalloidin/muscles; green, Hoechst/nuclei. Dashed light blue boxes indicate the disrupted single-file nuclear-positioning phenotype. Scale bar: 25 µm. *Twist-GAL4*/*apRed; DMef2-GAL4*/*apRed* was used as a control. (F) The ratio of actual internuclear distance to maximal internuclear distance in larval muscles from the indicated genotypes. Data points indicate the average value for the internuclear distance ratio for all nuclei within a single VL3 muscle. Error bars indicate the s.d. from 24 VL3 muscles. (G) The distance between nuclei and the nearest muscle edge in larval muscles from the indicated genotypes. Data points indicate the average distance from the muscle edge for all nuclei within a single VL3 muscle. Error bars indicate s.d. from 24 VL3 muscles. (H) Left, overlay immunofluorescence images of nuclei in VL3 muscles from dissected L3 larvae of the indicated genotype. Gray, Klarsicht; green, Hoechst/nuclei. Scale bar: 10 µm. Middle and right, grayscale images of Klarsicht (middle) and Hoechst/nuclei (right). (I) Intensity ratio for average Klarsicht immunofluorescence, with background fluorescence subtracted, normalized to the maximum Hoechst immunofluorescence and nuclear size. Error bars indicate s.d. from 20 nuclei. n.s., not significant ($P$>0.05), *$P$<0.05, **$P$<0.01, ***$P$<0.001, ****$P$<0.0001 compared to controls (Student's $t$-test).

Journal of Cell Science (2019) 132, jcs235580. doi:10.1242/jcs.235580

between shorter nesprin isoforms that localize to the inner nuclear membrane and function independently of the LINC complex (Mislow et al., 2002; Wheeler et al., 2007). In cell culture, emerin interacts with SUN proteins (Haque et al., 2010), but they do not rely on each other for nuclear envelope localization. If Bocksbeutel is not necessary for Klaroid localization, the decrease in nuclear-localized Klarsicht may be caused by LINC complex instability, possibly through lamins, which have been shown to be disrupted in large polytene nuclei that lack Bocksbeutel (Barton et al., 2014). In support of this, *bocksbeutel* expression was increased in *koi* mutants, perhaps to compensate for the loss of *koi*. Nevertheless, these data suggest that a loss of Klarsicht from the nuclear envelope is a driving factor of mispositioned myonuclei in *bocks*, *klar* and *koi* mutants. In support of this, the $klar^{1/Df}$ mutant (Fig. S1A–G) and muscle-specific knockdown of *klar* by RNAi (Collins et al., 2017) phenocopy $bocks^{DP01391}$ mutants, $klar^{1}$ mutants and $koi^{EY03560}$ mutants with the clustering phenotype in embryonic muscles and the single file nuclear-positioning phenotype in larval muscles. Furthermore, KASH-domain protein levels, such as Klarsicht, at the nucleus being a driving factor of mispositioned nuclei may not be unique to EDMD as Nesprin-1 levels at the nucleus have also been found to be reduced in the MDX mouse model for Duchenne muscular dystrophy (Iyer et al., 2017).

The increased amount of Klar at the nuclear envelope in *ote* mutants, and the associated nuclear-positioning phenotype, suggest that any variations in Klarsicht abundance at the nuclear envelope will impact nuclear position in muscle. Consistent with this, overexpression of Klarsicht in a muscle-specific manner phenocopied larval nuclear positioning relative to the muscle edge (Fig. 5A–C). Additionally, as an increase in Klarsicht leads to mispositioned nuclei, an increase in Klaroid has also been demonstrated to disrupt nuclear positioning (Tan et al., 2018). These data suggest that misregulation of LINC complex components that lead to a change in protein levels at the nucleus may be a common mechanism through which nuclear position is disrupted.

Remarkably, we found that loss of Otefin was sufficient to rescue the nuclear-positioning phenotypes present in $bocks^{DP01391}$ homozygous mutants, including both nuclear-localized Klarsicht levels and nuclear positioning. Furthermore, even the introduction of a single $ote^{DB}$ mutant allele was able to partially rescue nuclear positioning in $bocks^{DP01391}$ homozygous mutants, indicating the distinct emerin functions divided between the two *Drosophila emerin* homologs, *bocksbeutel* and *otefin*, must be balanced for proper nuclear positioning.

Taken together, these data suggest that nuclear positioning can be disrupted not only by the loss of LINC complex components but also increases in LINC complex components. Emerin is a critical regulator of LINC complex levels in the nucleus. Both the expression of Klarsicht and the localization of Klarsicht are regulated by emerin. However, we found here that in *Drosophila*, these two functions are divided among the two *Drosophila emerin* homologs, *bocksbeutel* and *otefin*. Thus, the specification of emerin activity may be the critical determinant of nuclear position and function. Given the functions of emerin in mechanosignaling (Guilluy and Burridge, 2015), genome organization (Boyle et al., 2001) and autophagy (Deroyer et al., 2014) among other functions the division of different emerin activities between *bocksbeutel* and *otefin* could serve as a valuable tool to further study emerin functions.

## MATERIALS AND METHODS

### *Drosophila* genetics

All stocks were grown under standard condition at 25°C. Stocks used were *apRed* which expresses *DsRed* fused to a nuclear localization signal downstream of the *apterous* mesodermal enhancer (Richardson et al., 2007), $bocks^{DP01391}$ (21846; Bloomington *Drosophila* Stock Center), $klar^{1}$ (3256; Bloomington *Drosophila* Stock Center), $ote^{DB}$ (5092; Bloomington *Drosophila* Stock Center), $koi^{EY03560}$ (20000; Bloomington *Drosophila* Stock Center), *bocks* deficiency Df(3R)Exel6153 (7632; Bloomington *Drosophila* Stock Center), *klar* deficiency Df(3L)BSC247 (9721, Bloomington *Drosophila* Stock Center), *ote* deficiency Df(2R)BSC337 (24361; Bloomington *Drosophila* Stock Center), *koi* deficiency Df(2R)Exel6050 (7532, Bloomington *Drosophila* Stock Center and UAS-*klar.6Xmyc*; derived from stock 25668; Bloomington *Drosophila* Stock Center) and $ote^{B279}$ (16189, Bloomington *Drosophila* Stock Center). Mutants were balanced and identified using *CyO*, *Dfd-GMR-nvYFP* and *TM6b, Dfd-GMR-nvYFP*. UAS-*klar.6Xmyc* was driven specifically in muscle using *DMEf2-GAL4*, *apRed*. The *twist-GAL4*, *apRed* and *Dmef2-GAL4*, *apRed Drosophila* lines were both used as controls. Third chromosome alleles have *twist-GAL4*, *apRed* on the second chromosome and second chromosome alleles have *Dmef2-GAL4*, *apRed* on the third chromosome to allow visualization of nuclei within the LT muscles during embryonic stages. Because there are slight variations between these two genotypes, each was used as a control. The *twist-GAL4*, *apRed* and *Dmef2-GAL4*, *apRed Drosophila* lines were made by recombining the *apRed* transgene and the specific GAL4 driver.

### Immunohistochemistry

Embryos were collected at 25°C and then dechorionated by submersion in 50% bleach for 4 min. Embryos were then washed with water and then fixed in 50% formalin (HT501128; Sigma-Aldrich) diluted in 1:1 with heptane and placed on an orbital shaker that rotated at a rate of 250 rpm for 20 min. In all cases, embryos were devitellinized by vortexing in a 1:1 methanol: heptane solution. Embryos were stored in methanol at −20°C until immunostaining.

Larvae were dissected as previously described (Metzger et al., 2012; Louis et al., 2008) with minor modifications. Larvae were dissected in ice-cold 1,4-piperazinediethanesulfonic acid (PIPES) dissection buffer containing 100 mM PIPES (P6757; Sigma-Aldrich), 115 mM D-sucrose (BP220-1; Thermo Fisher Scientific), 5 mM trehalose (182550250; Acros Organics), 10 mM sodium bicarbonate (BP328-500; Thermo Fisher Scientific), 75 mM potassium chloride (P333-500; Thermo Fisher Scientific), 4 mM magnesium chloride (M1028; Sigma-Aldrich) and 1 mM ethylene glycol tetraacetic acid (28-071-G; Thermo Fisher Scientific) and then fixed with 10% formalin for 20 min.

Antibodies for embryo staining were used at the following final dilutions: rabbit anti-dsRed, 1:400 (632496; Clontech); rat anti-tropomyosin, 1:200 (ab50567; Abcam), and mouse anti-green fluorescent protein, 1:50 (GFP-G1; Developmental Studies Hybridoma Bank). Antibodies for larval staining were used at the following final dilutions: mouse anti-Klar, 1:25 (KLAR-C 9E10; Developmental Studies Hybridoma Bank), mouse anti-LamC, 1:20 (LC28.26, Developmental Studies Hybridoma Bank), mouse anti-Myc, 1:200 (9B11, Cell Signaling Technology). Conjugated fluorescent secondary antibodies used for embryo staining were Alexa Fluor 555 donkey anti-rabbit-IgG (1:200), Alexa Fluor 488 donkey anti-rat-IgG (1:200) and Alexa Fluor 647 donkey anti-mouse-IgG (1:200; all Life Technologies). Alexa Fluor donkey anti-mouse-IgG (1:200; Life Technologies), Acti-stain 555-conjugated phalloidin (1:400; PHDH1-A; Cytoskeleton) and Hoechst 33342 (1 µg/ml; H3570; Life Technologies) were used for larval staining. Embryos and larvae were mounted in ProLong Gold (P36930; Life Technologies) and imaged with an Apochromat 40×/1.4 numerical aperture (NA) objective with a 1.0× optical zoom for all embryo images on a Zeiss 700 LSM. Larvae were imaged using the same microscope and objective lens at 0.5× optical zoom for nuclear positioning analysis and 2.0× optical zoom for Klarsicht localization, Hoechst intensity analysis and Myc-tagged Klarsicht localization.

Journal of Cell Science (2019) 132, jcs235580. doi:10.1242/jcs.235580

### Analysis of nuclear position in embryos

The position of nuclei was measured in stage 16 embryos, which is the latest stage before cuticle development blocks the ability to perform immunofluorescence microscopy. Embryos were staged primarily by gut morphology as previously described (Folker et al., 2012). Images acquired as described above were processed as maximum intensity projections of confocal *z*-stacks using ImageJ. The positioning of the nuclei was measured using the line function in ImageJ to determine the distance between either the dorsal end of the muscle and the nearest nucleus or the ventral end of the muscle and the nearest nucleus. All four LT muscles were measured in three or four hemisegments from each embryo. At least 20 embryos from at least two independent experiments were measured for each genotype, with the exception of experiments investigating mutants crossed to deficiencies, with each data point representing the average for all muscles measured within a single embryo. For experiments investigating mutants crossed to deficiencies, at least seven embryos from at least two independent experiments were measured. Statistical analysis was performed with Prism 4.0. Student's *t*-test was used to assess the statistical significance of differences in measurements between experimental genotypes and controls.

For qualitative nuclear-positioning phenotype analysis, embryos were scored on how nuclei positioned themselves within the first three LT muscles of three or four hemisegments in at least 20 embryos from at least two independent experiments, with the exception of experiments investigating mutants crossed to deficiencies. For experiments investigating mutants crossed to deficiencies at least seven embryos from at least two independent experiments were measured. LT4 was excluded for this analysis due to its variable muscle morphology. Nuclei were categorized as 'separated (equal distribution)' to indicate that nuclei were properly segregated into two distinct even clusters with a dorsal:ventral cluster area ratio >0.6 and <1.4, 'separated (unequal distribution)' to indicate that nuclei were separated into two distinct clusters that were uneven in size with a dorsal:ventral cluster area ratio of <0.6 or >1.4, 'central' to indicate that a nucleus or small cluster of nuclei was located in the middle of the myofiber that is not associated with either the dorsal or ventral cluster, 'clustered' to indicate that nuclei remain in a single cluster toward the ventral end of the myofiber, or 'spread' to indicate that nuclei are distributed along the myofiber with no distinct dorsal or ventral cluster. For the distinction of separated (equal distribution) and separated (unequal distribution), the areas of dorsal and ventral clusters were measured from each LT muscle using ImageJ. The nuclear distribution ratio was calculated by dividing the dorsal areas by the ventral areas. Statistical analysis was performed with Prism 4.0. Student's *t*-test was used to assess the statistical significance of differences in measurements between experimental genotypes and controls.

### Analysis of nuclear position in larvae

We measured nuclear position in larvae with our previously described method (Collins et al., 2017; Auld et al., 2018). First, the area and length of the muscle were measured. Next, the position and number of nuclei were calculated using the multipoint tool in ImageJ to place a point in the center of each nucleus. The position of each nucleus was used to calculate the actual internuclear distance. The maximal internuclear distance was then determined by taking the square root of the muscle area divided by the nuclear number. This value represents the distance between nuclei if their internuclear distance is fully maximized. The ratio between the actual internuclear distance and the maximal internuclear distance was then used to determine how evenly nuclei were distributed. This method normalizes the internuclear distance to both the nuclear count and the muscle area, which leads to a more representative means of comparison between muscles, larvae and genotypes. In addition, the distance of each nucleus from the lengthwise edge of the muscle was determined by measuring the shortest distance from the center of the nucleus to the nearest lengthwise edge of the muscle. A total of 24 ventral longitudinal (VL3) muscles were measured from at least six larvae with at least three VL3 muscles measured from each larva from at least two independent experiments. Statistical analysis was performed with Prism 4.0. Student's *t*-test was used to assess the statistical significance of differences in measurements between experimental genotypes and controls. The slope of the linear regression and $R^2$ values for the distance from muscle edge versus the average muscle width were determined using the linear regression function in Prism 4.0.

### Analysis of Klarsicht localization in larvae

Nuclear Klarsicht localization was measured in VL3 muscles of L3 larvae. *Z*-stack maximum projection images that extended through the entire nucleus were analyzed. The fluorescence intensity of Klarsicht and Hoechst were measured for the nucleus and the cytoplasm. The ratio between the background-subtracted average nuclear Klarsicht and maximum Hoechst fluorescence intensity was then used to determine the degree of Klarsicht localization at the nucleus while normalizing to Hoechst intensity to control for any staining variation between experiments (Fig. S5B,C). Since the EDMD-linked genes tested have an effect on nuclear size (Fig. S5A), the Hoechst normalized average nuclear Klarsicht fluorescence intensity ratio was also normalized to nuclear size. The Hoechst and size normalized intensity ratios were also normalized to the intensity ratios of control larvae that were dissected and stained on the same day using the same materials. A total of at least 20 nuclei were measured from at least six larvae from at least two independent experiments.

### Analysis of nuclear area, Hoechst integrated density and fluorescence intensities

Nuclear size, Hoechst integrated density, and mean and maximum fluorescence intensities were measured as previously described with minor modifications (Xiang et al., 2017; Wang et al., 2018). Briefly, individual nuclei in VL3 muscles were imaged as *Z*-stacks with 0.25 µm steps so as to image the entire nucleus. A low laser power was used to avoid saturation of the detectors, and imaging settings were kept constant throughout all nuclear size, Hoechst integrated density, and mean and maximum fluorescence intensity experiments. The nucleus was identified in ImageJ by converting the signals from the Lamin C fluorescence channel into a binary image, applying the 'fill holes' function and using the 'analyze particles' function with a size threshold set at >25 pixels resulting in selected regions of interest (ROI). The area of the ROI was recorded as the nuclear area. All slices from the Hoechst fluorescence channel were summed to create a projection of the nucleus, and a ROI from the Lamin C channel was selected in the Hoechst fluorescence channel using the restore selection function in ImageJ. The ROI in the Hoechst fluorescence channel was then measured for the mean and maximum Hoechst fluorescence intensities as well as the Hoechst integrated density.

### RT-qPCR

Gene expression was quantified by RT-qPCR. RNA was extracted and isolated from five L3 larvae by crushing in an Eppendorf tube in 1 ml of TRIzol according to the manufacturer's instructions (15596026, Invitrogen). A DNase I (04716728001; Sigma-Aldrich) digest was performed on the isolated RNA at 37°C for 30 min according to manufacturer's instructions. DNase I was inactivated through the addition of EDTA to a final concentration of 8 mM and heating to 75°C for 10 min. RNA integrity and concentrations were determined using the NanoDrop2000 system (Thermo Fisher Scientific). The cDNA library was established by performing reverse transcription using the SuperScript VILO cDNA synthesis kit (11-754-050; Invitrogen), according to the manufacturer's protocol. Briefly, purified RNA was incubated with SuperScript III reverse transcriptase at 42°C for 2 h and then reactions were terminated at 85°C for 5 min. The resulting cDNA was used as the template for qPCR using an ABI 7500 Fast real-time PCR system (Applied Biosystems) and Power SYBR green PCR Master Mix (4367659, Applied Biosystems) for detection. For each genotype, biological and technical triplicates were performed. Gene transcript levels were quantified using gene-specific primers designed using FlyPrimerBank (Hu et al., 2013) and primers were validated according to Applied Biosystems' instructions. The primers used were: *RP49* forward, 5′-GCCCAAGGGTATCGACAACA-3′; *RP49* reverse, 5′-GCGCTTGTTCGATCCGTAAC-3′; *GAPDH* forward, 5′-TAAATTCGACTCGACTCACGGT-3′; *GAPDH* reverse, 5′-CTCCAC-CACATACTCGGCTC-3′; *αTub84b* forward, 5′-GATCGTGTCCTCGAT-TACCGC-3′; *αTub84b* reverse, 5′-GGGAAGTGAATACGTGGGTAGG-3′; *bocks* forward, 5′-AGGACCAGCAGCCTAGACG-3′; *bocks* reverse,

5′-TCAACTTCGCGTGTGTAAGATG-3′; *klar* forward, 5′-GCGTGGGACAACTACCAAGA-3′; *klar* reverse, 5′-AATTCCAAGAGACGCCGGG-3′; *ote* forward, 5′-GATTCTCTGTCCAATGCTGAGTT-3′; *ote* reverse, 5′-TAGAACCTTCCGGCTGCTATC-3′; and *koi* forward, 5′-CTGACCTCGGACTATTCGAGC-3′; *koi* reverse, 5′-GGTGAGAATCGACGTGACTGT-3′. To confirm the effective removal of contaminating DNA and specificity of the primers, experiments were also conducted with reactions lacking reverse transcriptase. The differences in gene expression were calculated using the $\Delta\Delta C_t$ method. Rp49, GAPDH and αTub84b were used as the reference genes for comparison to the gene of interest for $\Delta C_t$ values for each sample. Fold changes were expressed as $2^{-\Delta\Delta Ct}$ and plotted in $Log_2$ for graphical representation. Statistical analysis was performed with Prism 4.0. Student's *t*-test was used to assess the statistical significance of differences in $\Delta C_t$ measurements between experimental genotypes and controls.

#### Acknowledgements
The authors would like to thank all members of the Folker lab for the helpful discussions in completing and interpreting these experiments.

#### Competing interests
The authors declare no competing or financial interests.

#### Author contributions
Conceptualization: E.S.F.; Methodology: T.R.M.; Formal analysis: T.R.M., B.D.T.; Investigation: T.R.M., B.D.T., A.J.A., M.R.H.; Resources: E.S.F.; Data curation: T.R.M.; Writing - original draft: T.R.M.; Writing - review & editing: E.S.F.; Supervision: E.S.F.; Project administration: E.S.F.; Funding acquisition: E.S.F.

#### Funding
This research was funded by a Scientist Development Grant from the American Heart Association to E.S.F. and by Boston College.

#### Supplementary information
Supplementary information available online at
http://jcs.biologists.org/lookup/doi/10.1242/jcs.235580.supplemental

#### References
**Ashery-Padan, R., Weiss, A. M., Feinstein, N. and Gruenbaum, Y.** (1997). Distinct regions specify the targeting of otefin to the nucleoplasmic side of the nuclear envelope. *J. Biol. Chem.* **272**, 2493-2499. doi:10.1074/jbc.272.4.2493

**Ashery-Padan, R., Ulitzur, N., Arbel, A., Goldberg, M., Weiss, A. M., Maus, N. A., Fisher, P. A. and Gruenbaum, Y.** (2015). Localization and posttranslational modifications of otefin, a protein required for vesicle attachment to chromatin, during Drosophila melanogaster development. *Mol. Cell. Biol.* **17**, 4114-4123. doi:10.1128/MCB.17.7.4114

**Auld, A. L., Collins, M. A., Mandigo, T. R. and Folker, E. S.** (2018). High-resolution imaging methods to analyze LINC complex function during Drosophila muscle development. *Methods Mol. Biol.* **1840**, 181-203. doi:10.1007/978-1-4939-8691-0_14

**Barton, L. J., Pinto, B. S., Wallrath, L. L. and Geyer, P. K.** (2013). The drosophila nuclear lamina protein otefin is required for germline stem cell survival. *Dev. Cell* **25**, 645-654. doi:10.1016/j.devcel.2013.05.023

**Barton, L. J., Wilmington, S. R., Martin, M. J., Skopec, H. M., Lovander, K. E., Pinto, B. S. and Geyer, P. K.** (2014). Unique and shared functions of nuclear lamina LEM domain proteins in Drosophila. *Genetics* **197**, 653-665. doi:10.1534/genetics.114.162941

**Bione, S., Maestrini, E., Rivella, S., Mancini, M., Regis, S., Romeo, G. and Toniolo, D.** (1994). Identification of a novel X-linked gene responsible for Emery-Dreifuss muscular dystrophy. *Nat. Genet.* **8**, 323-327. doi:10.1038/ng1294-323

**Boyle, S., Gilchrist, S., Bridger, J. M., Mahy, N. L., Ellis, J. A. and Bickmore, W. A.** (2001). The spatial organization of human chromosomes within the nuclei of normal and emerin-mutant cells. *Hum. Mol. Genet.* **10**, 211-219. doi:10.1093/hmg/10.3.211

**Cai, M., Huang, Y., Ghirlando, R., Wilson, K. L., Craigie, R. and Clore, G. M.** (2001). Solution structure of the constant region of nuclear envelope protein LAP2 reveals two LEM-domain structures: one binds BAF and the other binds DNA. *EMBO J.* **20**, 4399-4407. doi:10.1093/emboj/20.16.4399

**Collins, M. A., Mandigo, T. R., Camuglia, J. M., Vazquez, G. A., Anderson, A. J., Hudson, C. H., Hanron, J. L. and Folker, E. S.** (2017). Emery–Dreifuss muscular dystrophy-linked genes and centronuclear myopathy–linked genes regulate myonuclear movement by distinct mechanisms. *Mol. Biol. Cell* **28**, 2303-2317. doi:10.1091/mbc.e16-10-0721

**Crisp, M., Liu, Q., Roux, K., Rattner, J. B., Shanahan, C., Burke, B., Stahl, P. D. and Hodzic, D.** (2006). Coupling of the nucleus and cytoplasm: Role of the LINC complex. *J. Cell Biol.* **172**, 41-53. doi:10.1083/jcb.200509124

**Deroyer, C., Rénert, A.-F., Merville, M.-P. and Fillet, M.** (2014). New role for EMD (emerin), a key inner nuclear membrane protein, as an enhancer of autophagosome formation in the C16-ceramide autophagy pathway. *Autophagy* **10**, 1229-1240. doi:10.4161/auto.28777

**Ding, Z.-Y., Wang, Y.-H., Huang, Y.-C., Lee, M.-C., Tseng, M.-J., Chi, Y.-H. and Huang, M.-L.** (2017). Outer nuclear membrane protein Kuduk modulates the LINC complex and nuclear envelope architecture. *J. Cell Biol.* **216**, 2827-2841. doi:10.1083/jcb.201606043

**Dubowitz, V., Sewry, C. A. and Lane, R.** (2007). Definition of pathological changes seen in muscle biopsies. In *Muscle Biopsy: A Practical Approach*, pp 231-358. Philadephia, PA: Elsevier Limited.

**Elhanany-Tamir, H., Yu, Y. V., Shnayder, M., Jain, A., Welte, M. and Volk, T.** (2012). Organelle positioning in muscles requires cooperation between two KASH proteins and microtubules. *J. Cell Biol.* **198**, 833-846. doi:10.1083/jcb.201204102

**Folker, E. S. and Baylies, M. K.** (2013). Nuclear positioning in muscle development and disease. *Front. Physiol.* **4**, 363. doi:10.3389/fphys.2013.00363

**Folker, E. S., Schulman, V. K. and Baylies, M. K.** (2012). Muscle length and myonuclear position are independently regulated by distinct Dynein pathways. *Development* **139**, 3827-3837. doi:10.1242/dev.079178

**Guilluy, C. and Burridge, K.** (2015). Nuclear mechanotransduction: Forcing the nucleus to respond. *Nucleus* **6**, 19-22. doi:10.1080/19491034.2014.1001705

**Gundersen, G. G. and Worman, H. J.** (2013). Nuclear positioning. *Cell* **152**, 1376-1389. doi:10.1016/j.cell.2013.02.031

**Haque, F., Mazzeo, D., Patel, J. T., Smallwood, D. T., Ellis, J. A., Shanahan, C. M. and Shackleton, S.** (2010). Mammalian SUN protein interaction networks at the inner nuclear membrane and their role in laminopathy disease processes. *J. Biol. Chem.* **285**, 3487-3498. doi:10.1074/jbc.M109.071910

**Holaska, J. M. and Wilson, K. L.** (2007). An emerin "Proteome": purification of distinct emerin-containing complexes from HeLa cells suggests molecular basis for diverse roles including gene regulation, mRNA splicing, signaling, mechanosensing, and nuclear architecture. *Biochemistry* **46**, 8897-8908. doi:10.1021/bi602636m

**Hu, Y., Sopko, R., Foos, M., Kelley, C., Flockhart, I., Ammeux, N., Wang, X., Perkins, L., Perrimon, N. and Mohr, S. E.** (2013). FlyPrimerBank: an online database for Drosophila melanogaster gene expression analysis and knockdown evaluation of RNAi reagents. *G3* **3**, 1607-1616. doi:10.1534/g3.113.007021

**Iyer, S. R., Shah, S. B., Valencia, A. P., Schneider, M. F., Hernández-Ochoa, E. O., Stains, J. P., Blemker, S. S. and Lovering, R. M.** (2017). Altered nuclear dynamics in MDX myofibers. *J. Appl. Physiol.* **122**, 470-481. doi:10.1152/japplphysiol.00857.2016

**Laguri, C., Gilquin, B., Wolff, N., Romi-Lebrun, R., Courchay, K., Callebaut, I., Worman, H. J. and Zinn-Justin, S.** (2001). Structural characterization of the LEM motif common to three human inner nuclear membrane proteins. *Structure* **9**, 503-511. doi:10.1016/S0969-2126(01)00611-6

**Lee, K. K., Haraguchi, T., Lee, R. S., Koujin, T., Hiraoka, Y. and Wilson, K. L.** (2001). Distinct functional domains in emerin bind lamin A and DNA-bridging protein BAF. *J. Cell Sci.* **114**, 4567-4573.

**Lombardi, M. L., Jaalouk, D. E., Shanahan, C. M., Burke, B., Roux, K. J. and Lammerding, J.** (2011). The interaction between nesprins and sun proteins at the nuclear envelope is critical for force transmission between the nucleus and cytoskeleton. *J. Biol. Chem.* **286**, 26743-26753. doi:10.1074/jbc.M111.233700

**Louis, M., Huber, T., Benton, R., Sakmar, T. P. and Vosshall, L. B.** (2008). Bilateral olfactory sensory input enhances chemotaxis behavior. *Nat. Neurosci.* **11**, 187-199. doi:10.1038/nn2031

**Manilal, S., Man, N., Sewry, C. A. and Morris, G. E.** (1996). The Emery – Dreifuss muscular dystrophy protein, emerin, is a nuclear membrane protein. *Hum. Mol. Genet.* **5**, 801-808. doi:10.1093/hmg/5.6.801

**Metzger, T., Gache, V., Xu, M., Cadot, B., Folker, E. S., Richardson, B. E., Gomes, E. R. and Baylies, M. K.** (2012). MAP and kinesin-dependent nuclear positioning is required for skeletal muscle function. *Nature* **484**, 120-124. doi:10.1038/nature10914

**Mislow, J. M. K., Holaska, J. M., Kim, M. S., Lee, K. K., Segura-Totten, M., Wilson, K. L. and McNally, E. M.** (2002). Nesprin-1α self-associates and binds directly to emerin and lamin A in vitro. *FEBS J.* **525**, 135-140. doi:10.1016/S0014-5793(02)03105-8

**Nagano, A., Koga, R., Ogawa, M., Kurano, Y., Kawada, J., Okada, R., Hayashi, Y. K., Tsukahara, T. and Arahata, K.** (1996). Emerin deficiency at the nuclear membrane in patients with Emery-Dreifuss muscular dystrophy. *Nat. Genet.* **12**, 254-259. doi:10.1038/ng0396-254

**Navarro, A. P., Collins, M. A. and Folker, E. S.** (2016). The nucleus is a conserved mechanosensation and mechanoresponse organelle. *Cytoskeleton* **73**, 59-67. doi:10.1002/cm.21277

**Pinto, B. S., Wilmington, S. R., Hornick, E. E. L., Wallrath, L. L. and Geyer, P. K.** (2008). Tissue-specific defects are caused by loss of the drosophila MAN1 LEM domain protein. *Genetics* **180**, 133-145. doi:10.1534/genetics.108.091371

**Richardson, B. E., Beckett, K., Nowak, S. J. and Baylies, M. K.** (2007). SCAR/WAVE and Arp2/3 are crucial for cytoskeletal remodeling at the site of myoblast fusion. *Development* **134**, 4357-4367. doi:10.1242/dev.010678

**Roman, W. and Gomes, E. R.** (2018). Nuclear positioning in skeletal muscle. *Semin. Cell Dev. Biol.* **82**, 51-56. doi:10.1016/j.semcdb.2017.11.005

**Starr, D. A. and Han, M.** (2002). Role of ANC-1 in tethering nuclei to the actin cytoskeleton. *Science* **298**, 406-409. doi:10.1126/science.1075119

**Tan, K. L., Haelterman, N. A., Kwartler, C. S., Regalado, E. S., Lee, P.-T., Nagarkar-Jaiswal, S., Guo, D.-C., Duraine, L., Wangler, M. F., University of Washington Center for Mendelian Genomics, Bamshad, M. J. et al.** (2018). Ari-1 regulates myonuclear organization together with parkin and is associated with aortic aneurysms. *Dev. Cell* **45**, 226-244.e8. doi:10.1016/j.devcel.2018.03.020

**Technau, M. and Roth, S.** (2008). The Drosophila KASH domain proteins Msp-300 and Klarsicht and the SUN domain protein klaroid have no essential function during oogenesis. *Fly* **2**, 82-91. doi:10.4161/fly.6288

**Wagner, N., Schmitt, J. and Krohne, G.** (2004). Two novel LEM-domain proteins are splice products of the annotated Drosophila melanogaster gene CG9424 (Bocksbeutel). *Eur. J. Cell Biol.* **82**, 605-616. doi:10.1078/0171-9335-00350

**Wagner, N., Kagermeier, B., Loserth, S. and Krohne, G.** (2006). The Drosophila melanogaster LEM-domain protein MAN1. *Eur. J. Cell Biol.* **85**, 91-105. doi:10.1016/j.ejcb.2005.10.002

**Wang, S., Stoops, E., Cp, U., Markus, B., Reuveny, A., Ordan, E. and Volk, T.** (2018). Mechanotransduction via the LINC complex regulates DNA replication in myonuclei. *J. Cell Biol.* **217**, jcb.201708137. doi:10.1083/jcb.201708137

**Wheeler, M. A., Davies, J. D., Zhang, Q., Emerson, L. J., Hunt, J., Shanahan, C. M. and Ellis, J. A.** (2007). Distinct functional domains in nesprin-1$\alpha$ and nesprin-2$\beta$ bind directly to emerin and both interactions are disrupted in X-linked Emery-Dreifuss muscular dystrophy. *Exp. Cell Res.* **313**, 2845-2857. doi:10.1016/j.yexcr.2007.03.025

**Wilkinson, F. L., Holaska, J. M., Zhang, Z., Sharma, A., Manilal, S., Holt, I., Stamm, S., Wilson, K. L. and Morris, G. E.** (2003). Emerin interacts in vitro with the splicing-associated factor, YT521-B. *Eur. J. Biochem.* **270**, 2459-2466. doi:10.1046/j.1432-1033.2003.03617.x

**Windner, S. E., Manhart, A., Brown, A., Mogilner, A. and Baylies, M. K.** (2019). Nuclear scaling is coordinated among individual nuclei in multinucleated muscle fibers. *Dev. Cell* **49**, 48-62.e3. doi:10.1016/j.devcel.2019.02.020

**Xiang, J., Bandura, J., Zhang, P., Jin, Y., Reuter, H. and Edgar, B. A.** (2017). EGFR-dependent TOR-independent endocycles support Drosophila gut epithelial regeneration. *Nat. Commun.* **8**, 15125. doi:10.1038/ncomms15125

**Zheng, R., Ghirlando, R., Lee, M. S., Mizuuchi, K., Krause, M. and Craigie, R.** (2000). Barrier-to-autointegration factor (BAF) bridges DNA in a discrete, higher-order nucleoprotein complex. *Proc. Natl. Acad. Sci. USA* **97**, 8997-9002. doi:10.1073/pnas.150240197

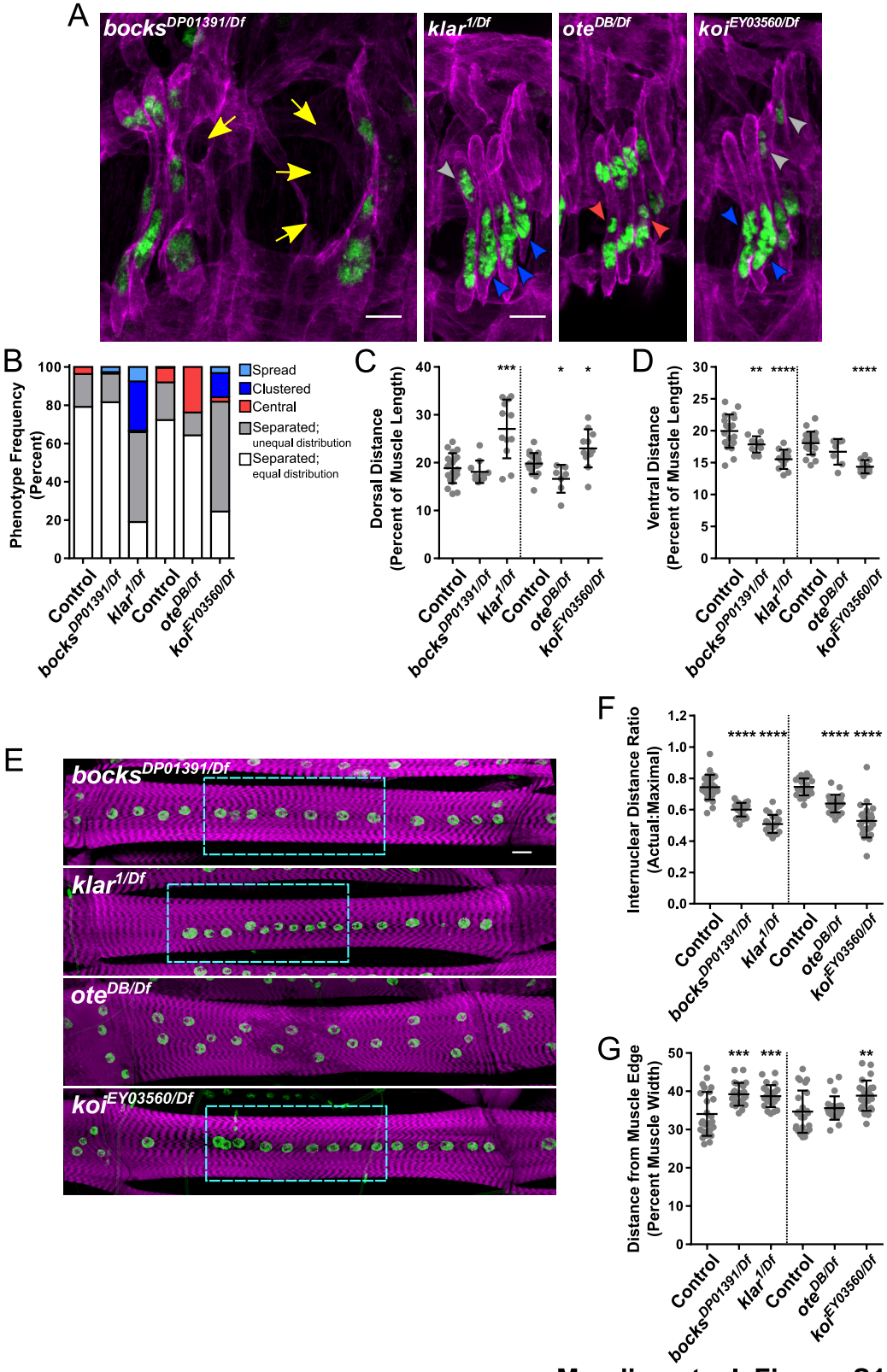


**Mandigo et. al. Figure. S1**

**Figure S1.** Analysis of EDMD-linked gene alleles in combination with deficiencies are consistent with the alleles affecting muscle development. (A) Immunofluorescence projection images of lateral transverse (LT) muscles in one hemisegment from stage 16 (16h AEL) embryos of indicated genotypes. Magenta, Tropomyosin/muscles; green, dsRed/nuclei. Yellow arrows indicate missing muscles. Arrowheads indicate disrupted nuclear positioning phenotypes. Dark Blue, clustered nuclear positioning; Gray, unequal separation of nuclear clusters; Red, central nuclei. Scale bar, 10 μm. (B) Qualitative analysis of the frequency at which nuclear positioning phenotypes occur in the indicated genotypes. (C,D) Distance between the dorsal end of the muscle and the nearest nucleus (C) and between the ventral end of the muscle and the nearest nucleus (D) for the indicated genotypes normalized to muscle length. Each data point represents the average distances from all measured muscles within a single embryo. Error bars indicate the SD from at least 7 embryos. (E) Immunofluorescence projection images of Ventral Longitudinal 3 (VL3) muscles from dissected L3 larvae of the indicated genotype. Magenta, phalloidin/ muscles; green, Hoechst/nuclei. Dashed boxes indicate disrupted nuclear positioning phenotypes; Light Blue, single file nuclei. Scale bar, 25 μm. (F) The ratio of actual internuclear distance to maximal internuclear distance in larval muscles from the indicated genotypes. Data points indicate the average value for the internuclear distance ratio for all nuclei within a single VL3 muscle. Error bars indicate the SD from 24 VL3 muscles. (G) The distance between nuclei and the nearest muscle edge in larval muscles from the indicated genotypes. Data points indicate the average distance from the muscle edge for all nuclei within a single VL3 muscle. Error bars indicate the SD from 24 VL3 muscles. Student's *t-test* were used for comparison to controls. *$p < 0.05$, **$p < 0.01$, ***$p < 0.001$, ****$p < 0.0001$.

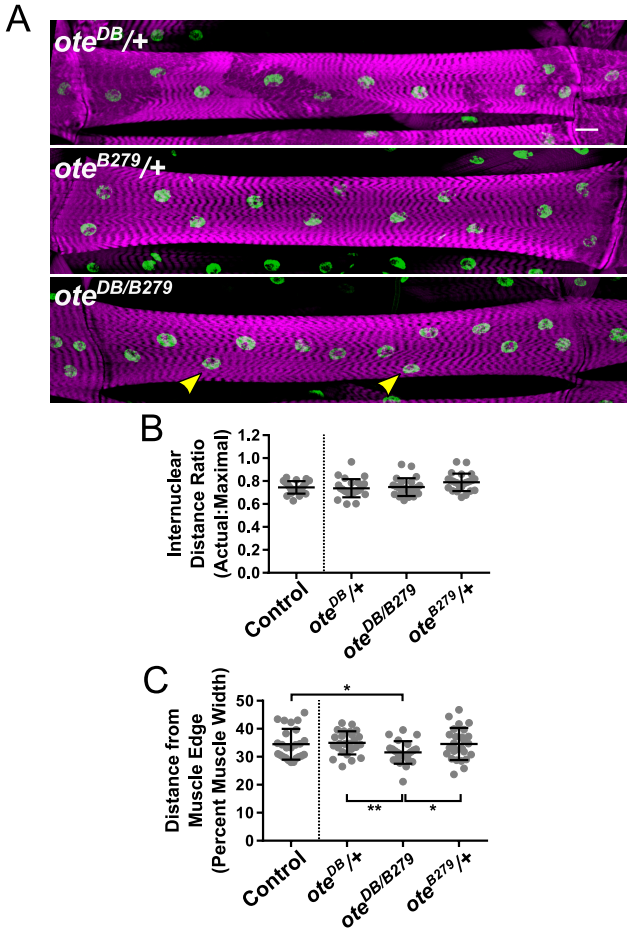


**Mandigo et. al. Figure. S2**

**Figure S2.** *otefin* trans-heterozygote phenocopies the *ote*$^{DB}$ homozygote with respect to nuclear positioning relative to the muscle edge. (A) Immunofluorescence projection images of VL3 muscles from dissected L3 larvae of the indicated genotype. Magenta, phalloidin/muscles; green, Hoechst/nuclei. Yellow arrowheads indicate nuclei that are closer to the muscle edge. Scale bar, 25 μm. (B) The ratio of actual internuclear distance to maximal internuclear distance in larval muscles from the indicated genotypes. Data points indicate the average value for the internuclear distance ratio for all nuclei within a single VL3 muscle. Error bars indicate the SD from 24 VL3 muscles. (C) The distance between nuclei and the nearest muscle edge in larval muscles from the indicated genotypes. Data points indicate the average distance from the muscle edge for all nuclei within a single VL3 muscle. Error bars indicate SD from 24 VL3 muscles. *$p < 0.05$, **$p < 0.01$.

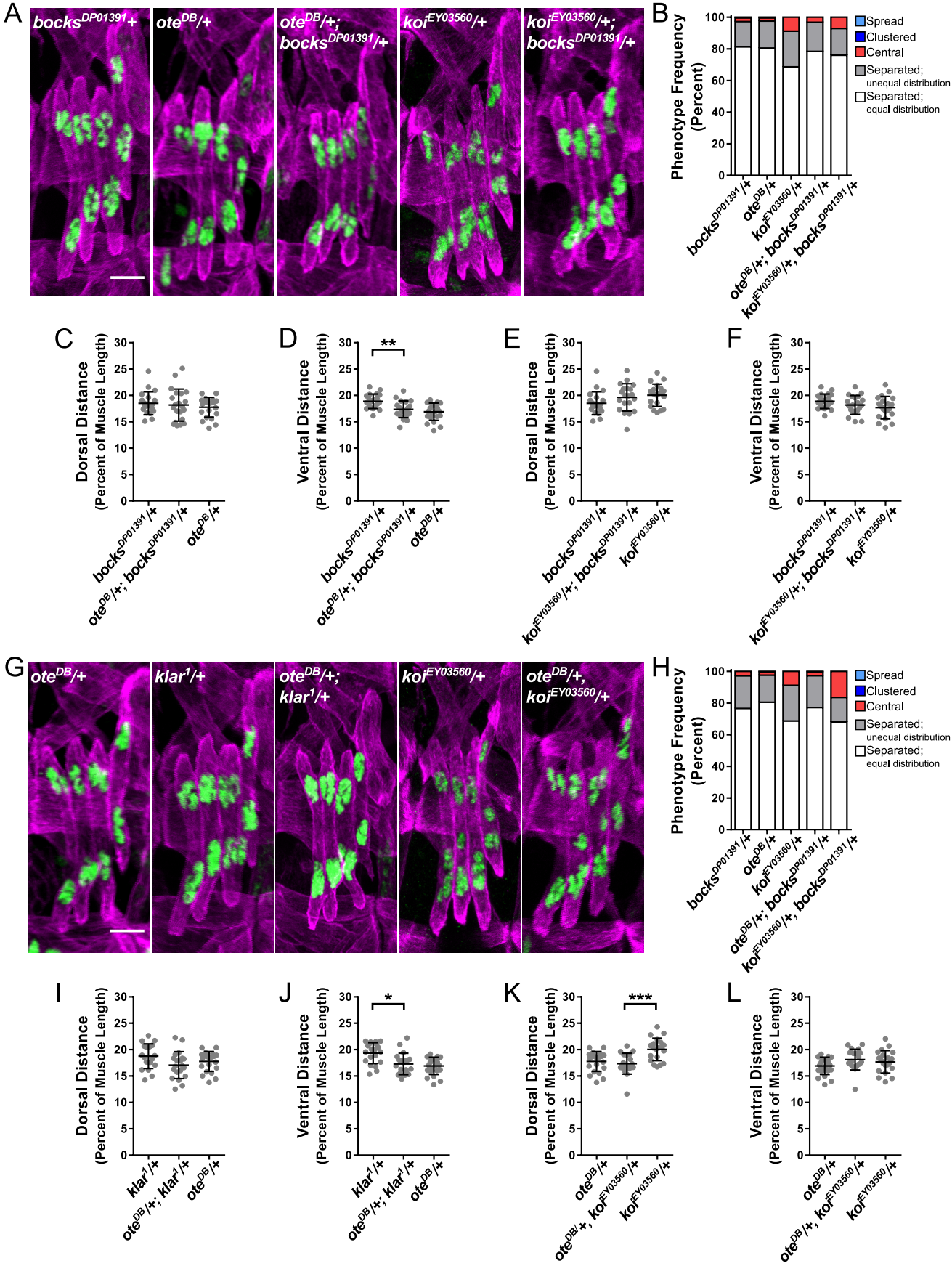


**Mandigo et. al. Figure S3**

**Figure S3.** *Bocksbeutel* does not genetically interact with *otefin* or *klaroid* and *otefin* does not genetically interact with *klarsicht* or *klaroid,* to regulate nuclear positioning in embryonic muscles. (A,G) Immunofluorescence projection images of LT muscles in one hemisegment from stage 16 (16h AEL) embryos with the indicated genotypes. Magenta, Tropomyosin/muscles; green, dsRed/nuclei. Scale bar, 10 μm. (B,H) Qualitative analysis of the frequency at which nuclear positioning phenotypes occur in the indicated genotypes. (C-F, I-L) Distance between the dorsal end of the muscle and the nearest nucleus (C,E,I,K) and between the ventral end of the muscle and the nearest nucleus (D,F,J,L) for the indicated genotypes normalized to muscle length. Each data point represents the average distance for all muscles measured within a single embryo. Error bars indicate the SD from 20 embryos. Student's *t-test* were used for comparison to controls. *p < 0.05, **p < 0.01, ***p < 0.001.

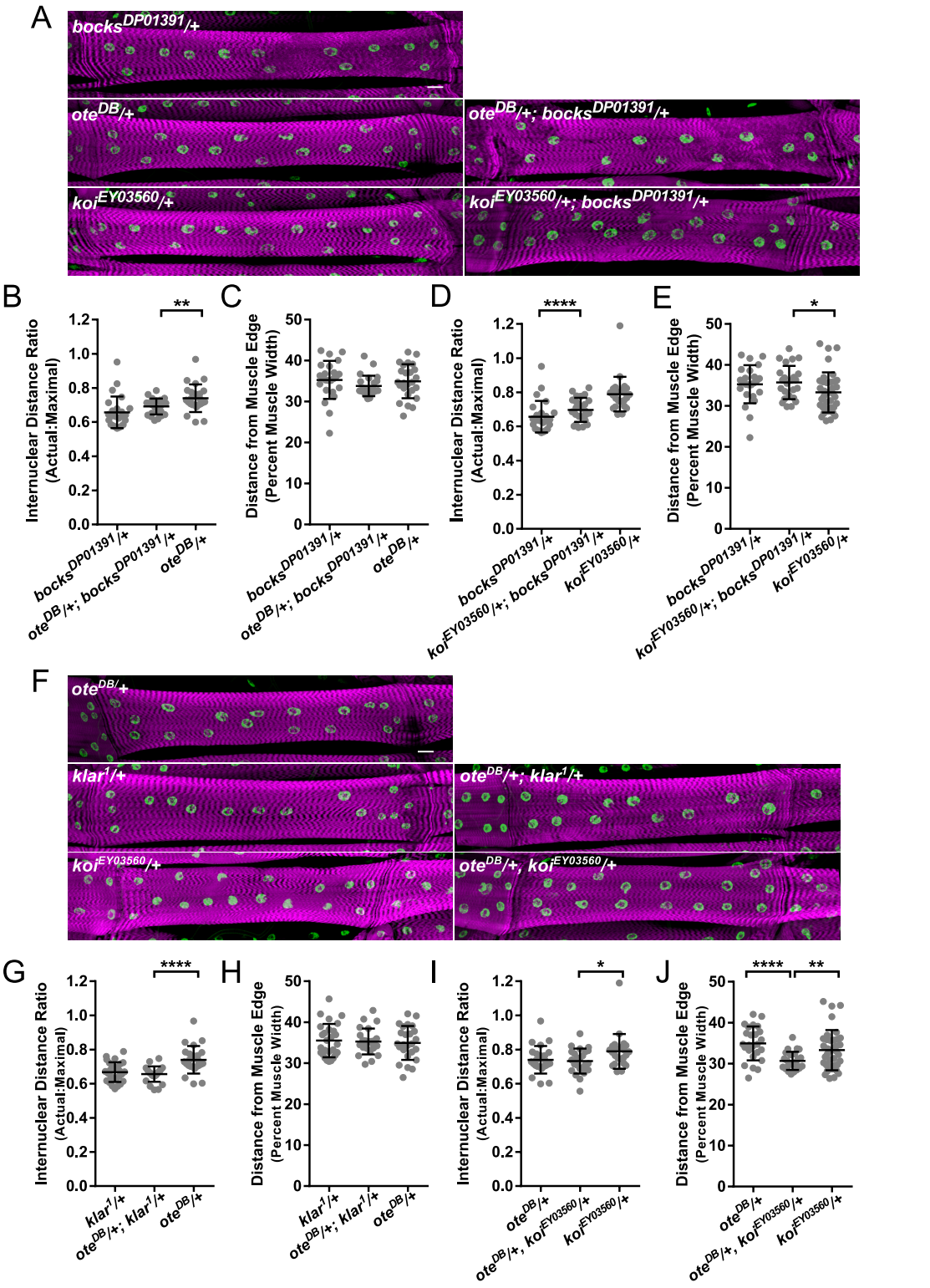


**Mandigo et. al. Figure S4**

**Figure S4.** *bocksbeutel* does not genetically interact with *otefin* or *klaroid* and *otefin* does not genetically interact with *klarsicht* or *klaroid* to regulate nuclear positioning in larval muscles. (A,F) Immunofluorescence projection images of VL3 muscles from dissected L3 larvae of the indicated genotype. Magenta, phalloidin/muscles; green, Hoechst/nuclei. Scale bar, 25 µm. (B,D,G,I) The ratio of actual internuclear distance to maximal internuclear distance in larval muscles from the indicated genotypes. Data points indicate the average value for the internuclear distance ratio for all nuclei within a single VL3 muscle. Error bars indicate the SD from 24 VL3 muscles. (C,E,H,J) The distance between nuclei and the nearest muscle edge in larval muscles from the indicated genotypes. Data points indicate the average distance from the muscle edge for all nuclei within a single VL3 muscle. Error bars indicate SD from 24 VL3 muscles. Student's *t-test* were used for comparison to controls. *$p < 0.05$, **$p < 0.01$, ****$p < 0.0001$.

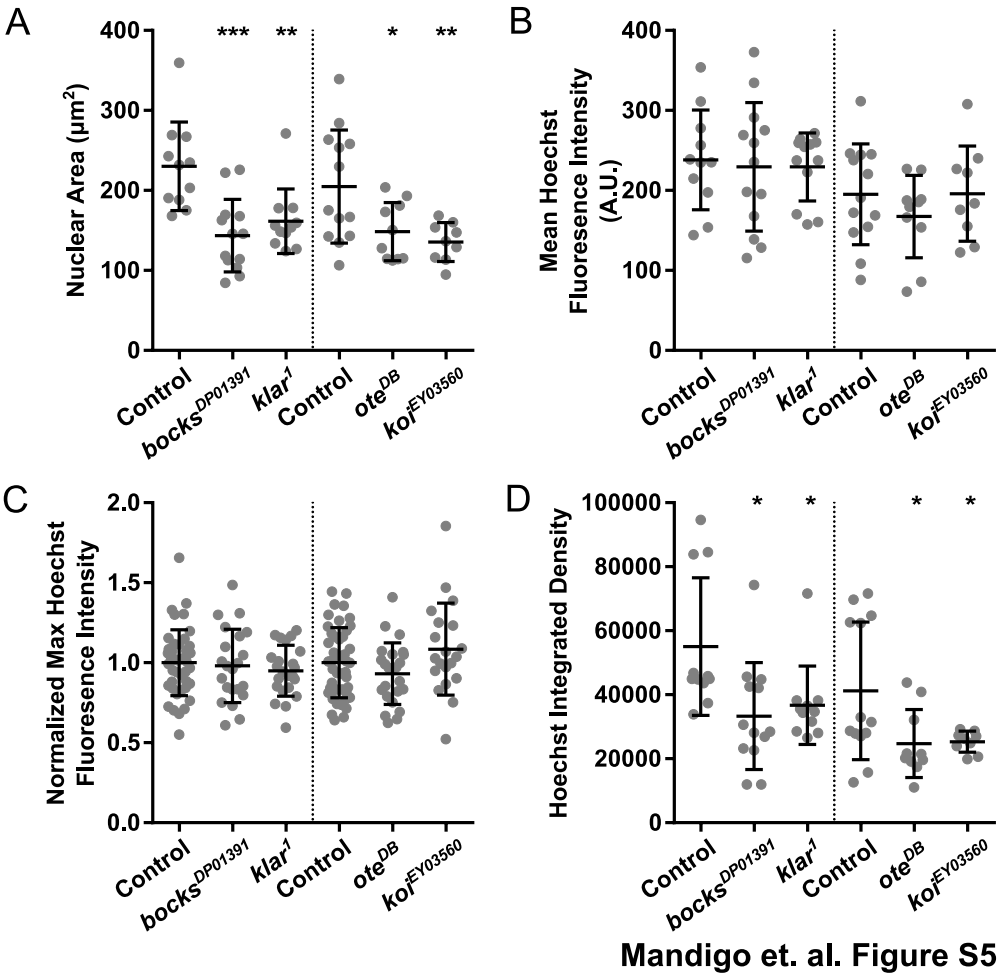

**Figure S5.** The EDMD-linked genes *bocksbeutel*, *klarsicht*, *otefin* and *klaroid* do not affect Hoechst intensity levels. (A,B,C,D)The nuclear area (A), mean Hoechst fluorescence intensity (B), maximum Hoechst fluorescence intensity normalized to control genotypes (C) and Hoechst integrated density (D) of the indicated genotypes. Data points indicate the measurements of a single nucleus. Error bars indicate the SD from at least 9 nuclei (A,B,D) or from at least 20 nuclei (C). Separate controls (*Twist-GAL4, apRed* (*first control*) and *DMef2-GAL4, apRed* (*second control*)) were used to control for variations caused by differences in genetic background. Student's *t-test* were used for comparison to controls. *p < 0.05, **p >0.01, ***p < 0.001.